Electronic Supplementary Material (ESI) for Journal of Materials Chemistry A.

Electronic supplementary information

Variable-valence ion and heterointerface accelerated electron transfer kinetics of electrochemical water splitting

Mengfei Lu[a, b], Shaoxi Kong[b], Shicheng Yan[b,*], Peng Zhou[b,*], Tao Yu[a,*], Zhigang Zou[a, b]

[a] Jiangsu Key Laboratory for Nano Technology, National Laboratory of Solid State Microstructures, School of Physics, Nanjing University, Nanjing, Jiangsu 210093, P. R. China.

[b] Jiangsu Key Laboratory of Artificial Functional Materials, Eco-materials and Renewable Energy Research Center (ERERC), Collaborative Innovation Center of Advanced Microstructures, College of Engineering and Applied Sciences, Nanjing University, Nanjing, Jiangsu 210093, P. R. China.

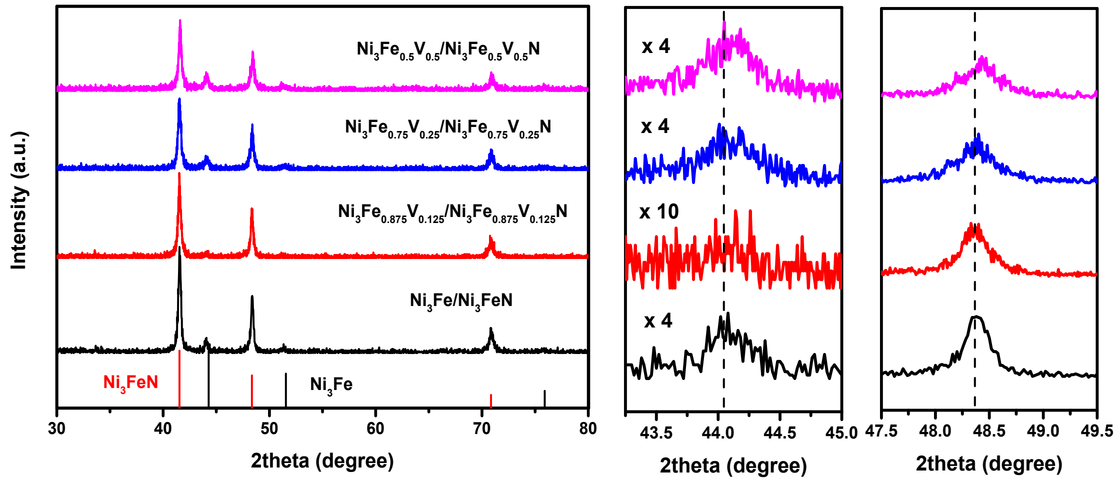

Fig. S1 XRD patterns of $Ni_3Fe_{1-X}V_X/Ni_3Fe_{1-X}V_XN$ (x = 0, 0.125, 0.25, 0.5) heterojunctions and enlarged regions at the 2theta of 43.25-45 and 47.5-49.5 degrees.

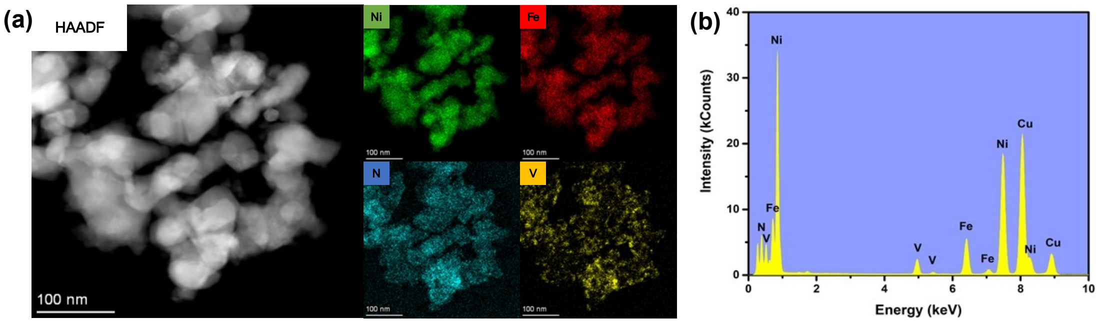

Fig. S2 (a) HAADF-STEM and (b) EDS elemental mapping images of $Ni_3Fe_{0.75}V_{0.25}/Ni_3Fe_{0.75}V_{0.25}N$.

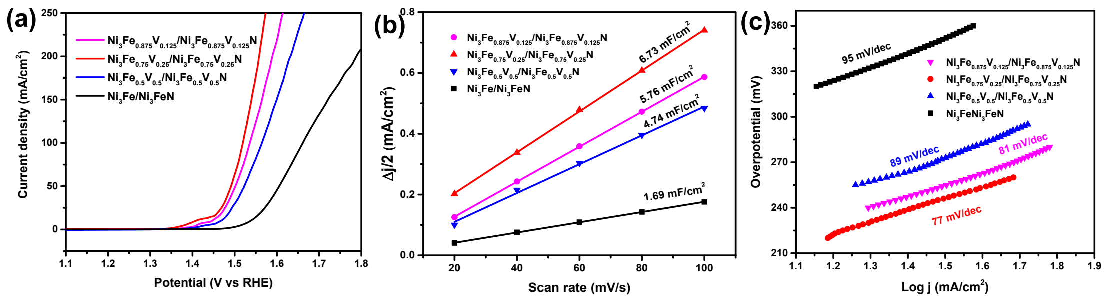

Fig. S3 The OER performances of $Ni_3Fe_{1-X}V_X/Ni_3Fe_{1-X}V_XN$ (x = 0, 0.125, 0.25, 0.5). (a) OER polarization curves with 90 % iR correction at a scan rate of 10 mV/s in 1.0 M KOH. (b) Plots of capacitive current density versus scan rate. The slopes (C_{dl}) represent ECSAs. (c) Tafel plots derived from the LSV data.

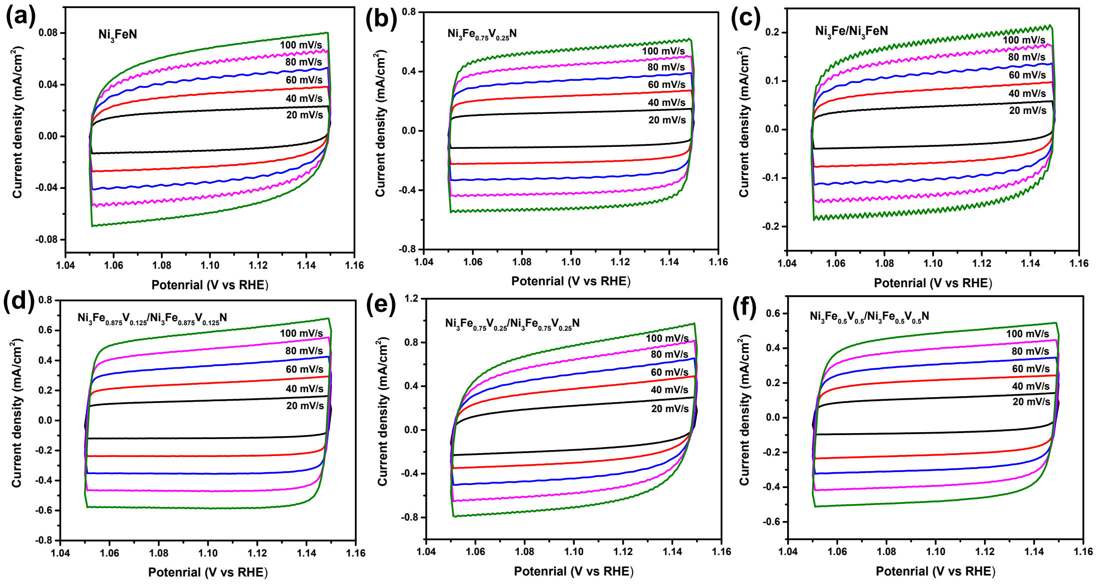

Fig. S4 Cyclic voltammetry curves of (a) Ni_3FeN, (b) $Ni_3Fe_{0.75}V_{0.25}N$, (c) Ni_3Fe/Ni_3FeN, (d) $Ni_3Fe_{0.875}V_{0.125}/Ni_3Fe_{0.75}V_{0.25}N$, (e) $Ni_3Fe_{0.75}V_{0.25}/Ni_3Fe_{0.75}V_{0.25}N$, and (d) $Ni_3Fe_{0.5}V_{0.5}/Ni_3Fe_{0.5}V_{0.5}N$ at various scan rates (20, 40, 60, 80 and 100 mV/s) in 1.0 M KOH.

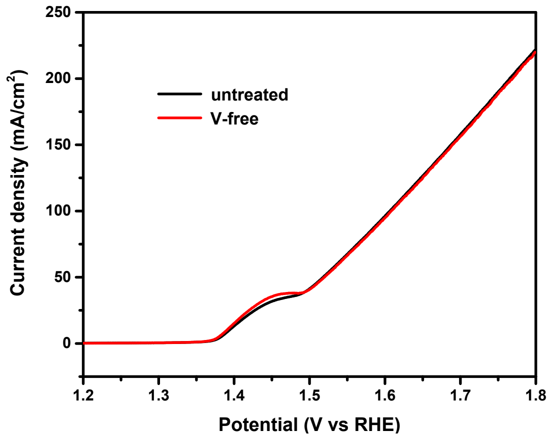

Fig. S5 The OER activities of $Ni_3Fe_{0.75}V_{0.25}/Ni_3Fe_{0.75}V_{0.25}N$ tested without iR correction in 1.0 M KOH solution with and without dissolved V ions.

To address the V-effect, the equal amount of fresh 1.0 M KOH solution was substituted after activating the samples, which was labeled as V-free. It can be seen from Fig. S5 that the activated $Ni_3Fe_{0.75}V_{0.25}/Ni_3Fe_{0.75}V_{0.25}N$ shows indistinguishable LSV curves for OER, indicating that the trace amount of dissolved V ions barely affected the assessment of electrocatalytic activities.

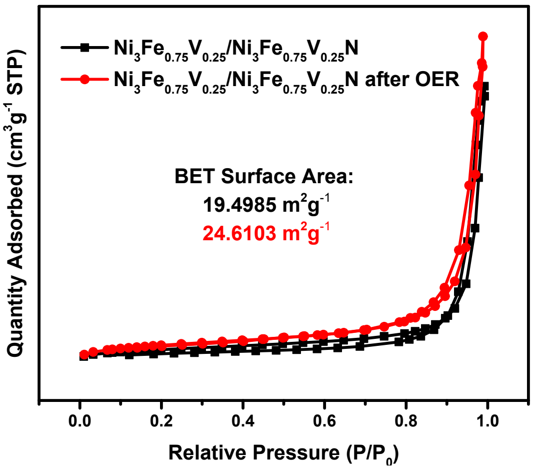

Fig. S6 N_2 adsorption-desorption isotherms and Brunauer-Emmett-Teller (BET) specific surface areas of $Ni_3Fe_{0.75}V_{0.25}/Ni_3Fe_{0.75}V_{0.25}N$ before and after OER.

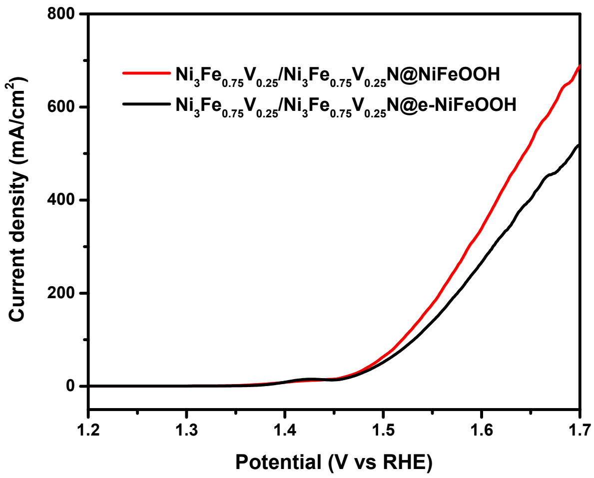

Fig. S7 The OER polarization curves of $Ni_3Fe_{0.75}V_{0.25}/Ni_3Fe_{0.75}V_{0.25}N$ with in-situ formed FeNi (oxy)hydroxide ($Ni_3Fe_{0.75}V_{0.25}/Ni_3Fe_{0.75}V_{0.25}N$@NiFeOOH) and eletrodeposited FeNi (oxy)hydroxide ($Ni_3Fe_{0.75}V_{0.25}/Ni_3Fe_{0.75}V_{0.25}N$@e-NiFeOOH).

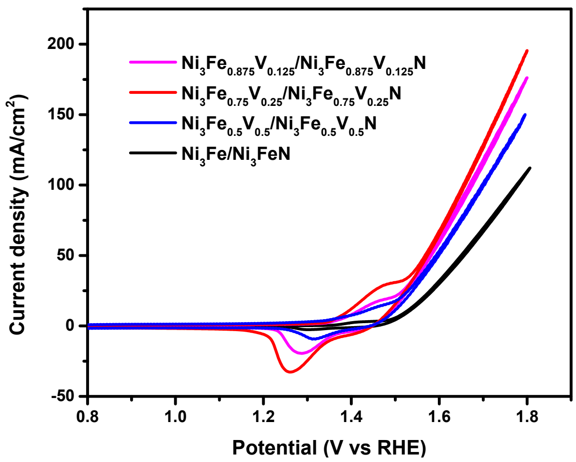

Fig. S8 CV curves of $Ni_3Fe_{1-x}V_x/Ni_3Fe_{1-x}V_xN$ (x = 0, 0.125, 0.25, 0.5) in 1.0 M KOH with a scan rate of 100 mV/s without iR compensation.

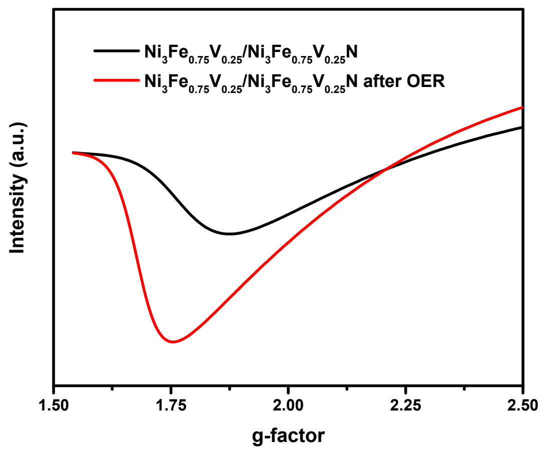

Fig. S9 The EPR spectra of $Ni_3Fe_{0.875}V_{0.125}/Ni_3Fe_{0.75}V_{0.25}N$ before and after OER.

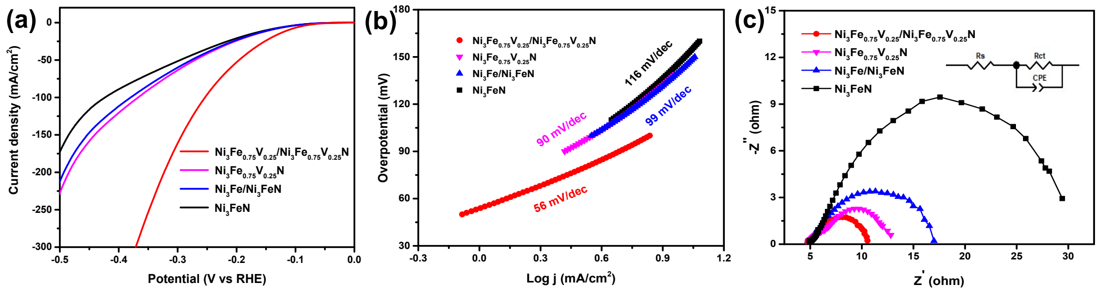

Fig. S10 The performances and properties of Ni_3FeN, $Ni_3Fe_{0.75}V_{0.25}N$, Ni_3Fe/Ni_3FeN, and $Ni_3Fe_{0.75}V_{0.25}/Ni_3Fe_{0.75}V_{0.25}N$ for HER. (a) HER polarization curves with 90% iR correction at a scan rate of 10 mV/s in 1.0 M KOH. (b) Tafel plots derived from the LSV data. (c) EIS Nyquist plots.

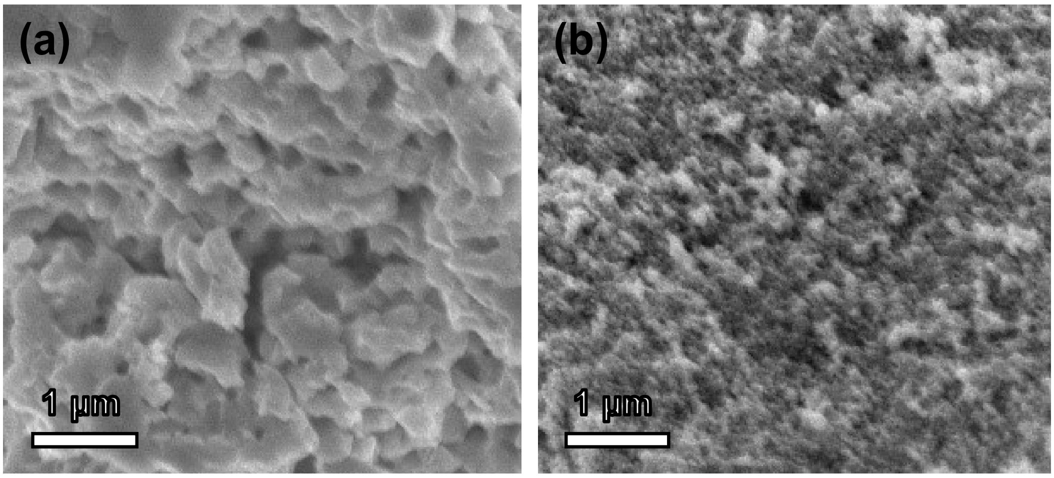

Fig. S11 SEM images of (a) as-prepared Ni_3Fe/Ni_3FeN and (b) $Ni_3Fe_{0.75}V_{0.25}/Ni_3Fe_{0.75}V_{0.25}N$.

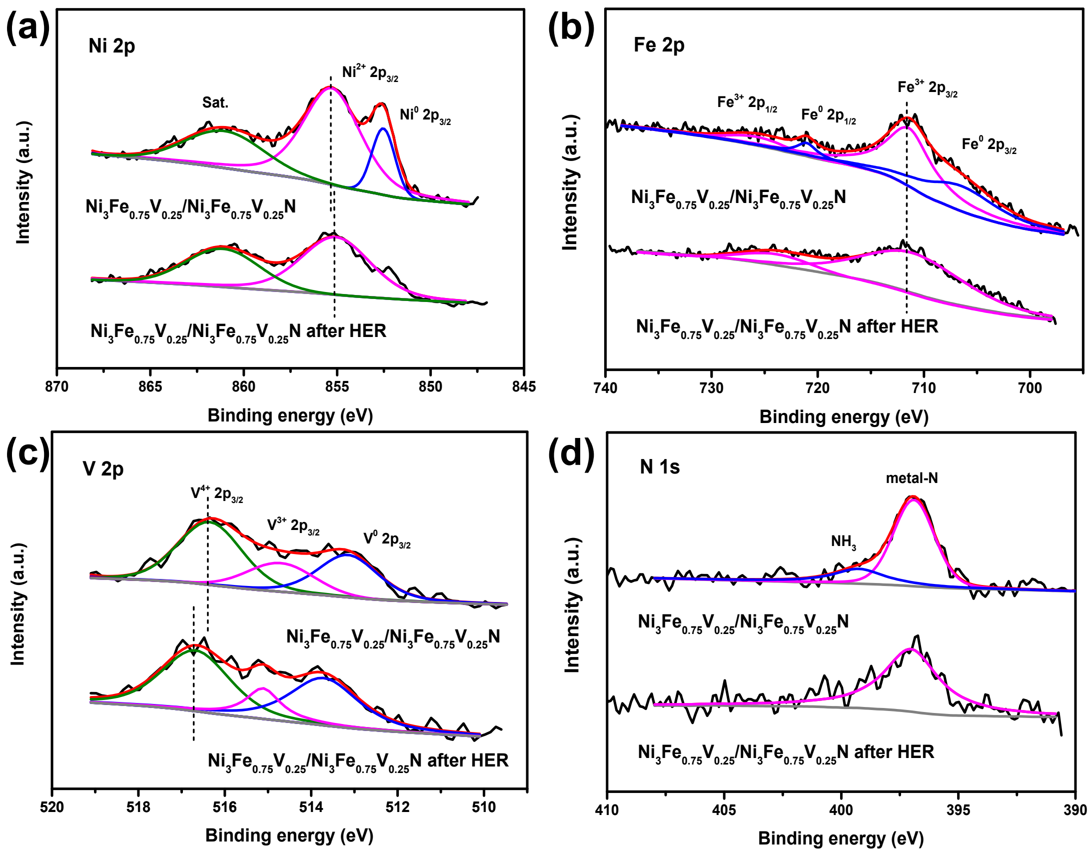

Fig. S12 XPS spectra of (a) Ni 2p, (b) Fe 2p, (c) V 2p and (d) N 1s for $Ni_3Fe_{0.75}V_{0.25}/Ni_3Fe_{0.75}V_{0.25}N$ before and after HER.

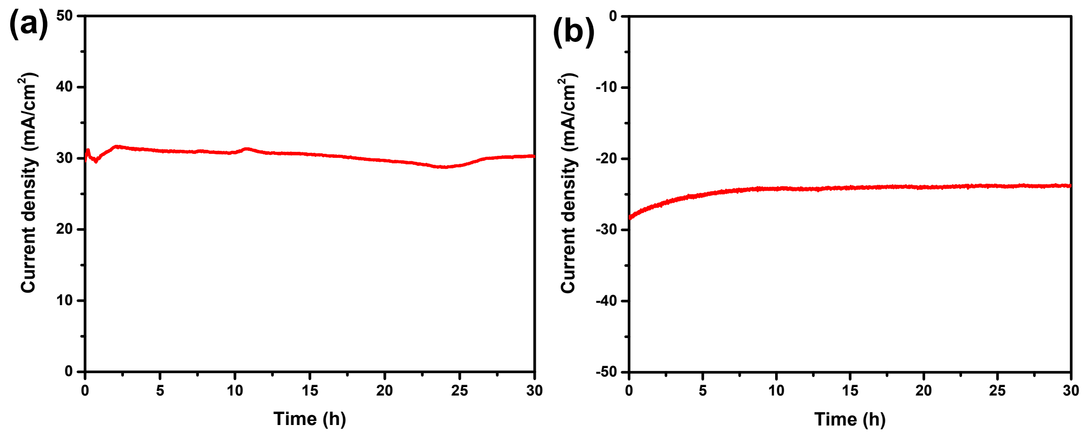

Fig. S13 Time-dependent stability of $Ni_3Fe_{0.75}V_{0.25}/Ni_3Fe_{0.75}V_{0.25}N$ for (a) OER and (b) HER at the applied potential of 1.5 V vs RHE and -0.3 V vs RHE, respectively.

Table S1 Compositions of the samples determined by ICP-AES.

Samples	The content of metal ions (mmol/L)			Mole ratio	
	Ni	Fe	V	Ni/(Fe+V)	V/Fe
Ni_3Fe/Ni_3FeN	5.844	1.987	/	2.94	/
$Ni_3Fe_{0.75}V_{0.25}/Ni_3Fe_{0.75}V_{0.25}N$	5.197	1.303	0.418	3.02	0.32
$Ni_3Fe_{0.75}V_{0.25}/Ni_3Fe_{0.75}V_{0.25}N$@NiFeOOH	4.481	1.067	0.129	3.75	0.12

Table S2 The OER and HER performances comparison of V-Ni3Fe/Ni3FeN with the alloy(metal)/nitrides composite electrocatalysts currently reported.

Samples	OER (mV)	HER (mV)	Reference
$Ni_3Fe_{0.75}V_{0.25}/Ni_3Fe_{0.75}V_{0.25}N$	261 (η_{50})	113 (η_{10})	this work
Ni_3Fe/Ni_3FeN	390 (η_{50})	166 (η_{10})	1
Ni_3Fe/Ni_3FeN	290 (η_{50})	--	2
Ni_3Fe/Ni_3FeN	295 (η_{50})	125 (η_{10})	3
Mo-Ni_3Fe/Ni_3FeN	340 (η_{50})	234 (η_{10})	4
Fe_3Pt/Ni_3FeN	365 (η_{10})	--	5
Ni/Ni_3FeN	255 (η_{50})	--	6
NiCu/NiCuN/NC	232 (η_{10})	93 (η_{10})	7
$FeCo/Co_4N/NC$	280 (η_{10})	--	8
WC/W_2N	320 (η_{10})	148.5 (η_{10})	9
Co_3W/WN	273 (η_{10})	43 (η_{10})	10
CoB_x@BN	290 (η_{10})	--	11

It was noted that the overpotential of Ni/Ni_3FeN@NiFeOOH reported in the reference 6 was a little smaller than the $Ni_3Fe_{0.75}V_{0.25}/Ni_3Fe_{0.75}V_{0.25}N$@NiFeOOH sample in this work, however, our catalysts presented much higher current density than Ni/Ni_3FeN@NiFeOOH at high potential.

Table S3 Fitting parameters of EIS plots for OER based on the Randle's equivalent circuit.

Samples	CPE/QPE		C_{ct}(mF)	R_{ct}(Ω)	R_s(Ω)
	P=n	T=Q^n			
Ni_3FeN	0.86	1.6161	0.228	122.9	6.941
Ni_3Fe/Ni_3FeN	0.89	3.4247	0.956	30.35	6.953
$Ni_3Fe_{0.75}V_{0.25}N$	0.89	9.2408	3.297	16.49	7.167
$Ni_3Fe_{0.875}V_{0.125}/Ni_3Fe_{0.875}V_{0.125}N$	0.75	21.946	1.862	14.57	6.568
$Ni_3Fe_{0.75}V_{0.25}/Ni_3Fe_{0.75}V_{0.25}N$	0.76	67.172	13.01	5.972	5.532
$Ni_3Fe_{0.5}V_{0.5}/Ni_3Fe_{0.5}V_{0.5}N$	0.86	12.026	3.141	10.96	5.635

Table S4 Fitting parameters of EIS plots for HER based on the Randle's equivalent circuit.

Samples	CPE/QPE		C_{ct}(mF)	R_{ct}(Ω)	R_s(Ω)
	P=n	T=Q^n			
Ni_3FeN	0.76	8.4979	0.420	26.24	5.531
Ni_3Fe/Ni_3FeN	0.63	14.344	0.048	12.78	5.056
$Ni_3Fe_{0.75}V_{0.25}N$	0.66	10.761	0.056	7.595	5.685
$Ni_3Fe_{0.75}V_{0.25}/Ni_3Fe_{0.75}V_{0.25}N$	0.67	18.577	0.228	5.821	5.115

The effective capacitance associated with the CPE can be calculated based on the equation:

$$C_{ct}= Q^{1/n}(1/R_s+1/R_{ct})^{(n-1)/n}$$

where the parameters of pre-factor (Q) and exponent (n) are independent of frequency. When n=1, Q represents the capacity of the interface; when n<1, the system behavior is related to the surface heterogeneity [12].

1. H. Li, S. Ci, M. Zhang, J. Chen, K. Lai and Z. Wen, *ChemSusChem*, 2017, **10**, 4756-4763.
2. X. Fu, J. Zhu, B. Ao, X. Lyu and J. Chen, *Inorg. Chem. Commun.*, 2020, **113**, 107802.
3. Z. Li, H. Jang, D. Qin, X. Jiang, X. Ji, M. G. Kim, L. Zhang, X. Liu and J. Cho, *J. Mater. Chem. A*, 2021, **9**, 4036-4043.
4. Z. Shao, J. Sun, Z. Yan, K. Huang, F. Tian, H. Xue and Q. Wang, *Appl. Surf. Sci.*, 2020, **529**, 147172.
5. Z. Cui, G. Fu, Y. Li and J. B. Goodenough, *Angew. Chem. Int. Ed. Engl.*, 2017, **56**, 9901-9905.
6. J. Wang, F. Cao, C. Shen, G. Li, X. Li, X. Yang, S. Li and G. Qin, *Catal. Sci. Technol.*, 2020, **10**, 4458-4466.
7. J. Hou, Y. Sun, Z. Li, B. Zhang, S. Cao, Y. Wu, Z. Gao and L. Sun, *Adv. Funct. Mater.*, 2018, **28**, 1803278.
8. X. Zhu, T. Jin, C. Tian, C. Lu, X. Liu, M. Zeng, X. Zhuang, S. Yang, L. He, H. Liu and S. Dai, *Adv. Mater.*, 2017, **29**, 1704091.
9. J. Diao, Y. Qiu, S. Liu, W. Wang, K. Chen, H. Li, W. Yuan, Y. Qu and X. Guo, *Adv. Mater.*, 2020, **32**, 1905679.
10. J. Zheng, J. Chen, L. Xiao, X. Cheng and H. Cui, *ChemElectroChem*, 2020, **7**, 4971-4978.
11. S. Chen, Y. Li, Z. Zhang, Q. Fu and X. Bao, *J. Mater. Chem. A*, 2018, **6**, 10644-10648.
12. B. Hirschorn, M. E. Orazem, B. Tribollet, V. Vivier, I. Frateur and M. Musiani, *Electrochim. Acta*, 2010, **55**, 6218-6227.

References